



Heterogeneous & Homogeneous & Bio- & Nano-

# CHEM**CAT**CHEM

  
**CATALYSIS**

## Accepted Article

**Title:** Mesoporous CoS/ N-doped Carbon as HER and ORR Bifunctional Electrocatalyst for Water Electrolysers and Zinc-Air Batteries

**Authors:** Jieting Ding, Shan Ji, Hui Wang, Bruno G. Pollet, and Rongfang Wang

This manuscript has been accepted after peer review and appears as an Accepted Article online prior to editing, proofing, and formal publication of the final Version of Record (VoR). This work is currently citable by using the Digital Object Identifier (DOI) given below. The VoR will be published online in Early View as soon as possible and may be different to this Accepted Article as a result of editing. Readers should obtain the VoR from the journal website shown below when it is published to ensure accuracy of information. The authors are responsible for the content of this Accepted Article.

**To be cited as:** *ChemCatChem* 10.1002/cctc.201801618

**Link to VoR:** <http://dx.doi.org/10.1002/cctc.201801618>

WILEY-VCH

[www.chemcatchem.org](http://www.chemcatchem.org)

A Journal of



## FULL PAPER

## WILEY-VCH

# Mesoporous CoS/ N-doped Carbon as HER and ORR Bifunctional Electrocatalyst for Water Electrolyzers and Zinc-Air Batteries

Jieting Ding,<sup>[a]</sup> Shan Ji,<sup>\*[b]</sup> Hui Wang,<sup>[a]</sup> Bruno G. Pollet<sup>[c]</sup> and Rongfang Wang<sup>\*[a]</sup>

**Abstract:** Hydrogen evolution reaction (HER) and oxygen reduction reaction (ORR) are two critical electrocatalytic reactions, involved in many sustainable and green electrochemical energy conversion and storage technologies. Transition metal-based compound combined with carbon materials have been found to be effective catalysts toward the HER and ORR with great potential to replace conventional precious metal-based catalysts. Herein, a low-cost method is described for the fabrication and testing of sulphide (CoS)/carbon compound with high specific surface area and mesoporous structure by using peptone as raw material and NaCl as template. The obtained materials showed open structures composed of interconnected thin carbon nanosheets with transition metal-based nanoparticles wrapped inside the carbon matrix. These as-prepared materials were used as HER and ORR bifunctional catalysts for water electrolysis and Zn-air battery. In the alkaline media, the optimized catalysts exhibited highly efficient electrocatalysis toward the HER. They also showed an outstanding ORR activity and durability which was found to be superior to commercial Pt/C catalysts. In an assembled primary Zn-air cell containing the optimized sample, the open circuit voltage (OCV) was 1.44 V, higher than the value for Zn-air cell containing Pt/C. The assembled Zn-air cell delivered a power density of 119 mW cm<sup>-2</sup> at 150 mA cm<sup>-2</sup>, higher than the Pt/C cell (97 mW cm<sup>-2</sup> at 150 mA cm<sup>-2</sup>).

## Introduction

The challenges of global warming, depleting fossil fuel resources and serious pollution that humans are being faced with, have stimulated considerable research efforts in the exploration of sustainable and green energy technologies, such as hydrogen and fuel cells, metal-air batteries and water splitting<sup>[1]</sup>. The key process of these sustainable and green energy conversion and storage technologies are a series of electrocatalytic reactions, for example, in water electrolysis, the hydrogen evolution reaction (HER) occurs at the cathode<sup>[2]</sup>, in a Zn-air battery, the oxygen reduction reaction (ORR) occurs at the air cathode<sup>[3]</sup> and in fuel cells, the ORR occurs at the

cathode<sup>[4]</sup>. Due to the sluggish kinetics of the HER and ORR, precious-metal based catalysts are required to reduce the overpotential ( $\eta$ ) and achieve high efficiency. However, the large-scale applications of these green technologies have been seriously impeded by the high-cost and scarcity of the precious group metals (PGM)<sup>[5]</sup>. To develop low-cost and alternatives to PGM-based catalysts, there has been a lot of research efforts and activities in durable non-precious metals for use in water electrolysis, fuel cells and zinc-air battery technologies.

Transition metal compounds, such as nitrides, sulphides, selenides, oxides, phosphides, have been found to be promising HER and ORR catalysts with great potential as alternatives to precious metal catalysts. For example, NiO/CoN nanowire arrays have been reported as good bifunctional catalysts, exhibiting acceptable electrocatalytic activity toward OER and ORR due to both oxygen vacancies and interfaces between CoN and NiO phases<sup>[6]</sup>. Asiri et al. reported a method to electrochemically deposit Ni<sub>3</sub>S<sub>2</sub> film on Cu foam as HER and OER bifunctional catalysts exhibiting good activity and durability in alkaline media<sup>[7]</sup>. Unfortunately, these newly developed transition metal compounds (TMC) still cannot compete with precious metal catalysts since the aggregation of the obtained TMC nanoparticles lead to poor stability and activity induced by the loss of active sites available on the surface<sup>[1a]</sup>. Recently, it was found that the electrocatalytic performance of TMC nanoparticles can be significantly enhanced when TMC are encapsulated in much stable materials with high surface areas, such as carbon nanotubes, graphene and porous carbon<sup>[8]</sup>. For example, Co encapsulated in carbon nanotubes exhibited high HER activity in alkaline electrolytes in a wide range of pH's<sup>[9]</sup>. Nitrogen-doped graphene containing Co nanoparticles have been successfully developed as OER and ORR bifunctional electrocatalysts by Liao<sup>[10]</sup>. Nanosized CuFe alloy entrapped within graphitic carbon was synthesized and used as a highly efficient and stable ORR electrocatalyst in alkaline solutions<sup>[11]</sup>. It was found that combining TMC and carbon materials together not only avoid particle aggregation, but also enhance electrocatalytic performance via the synergistic effect between carbon and TMC<sup>[2b]</sup>. In addition, the electrocatalytic properties of TMC/carbon materials can be further tuned and optimized by controllable synthesis of morphology and porosity of the carbon matrix<sup>[12]</sup>.

In this study, CoS nanoparticles encapsulated in mesoporous N-doped carbon (Co/NC) materials were synthesized and tested as HER and ORR bifunctional catalysts. Peptone was chosen as carbon and nitrogen sources to form the N-doped carbon and the NaCl salt was used as template to form the porous structure during the carbonizing process at high temperatures. Compared to the conventional templating method to generate mesoporous structure, this new synthesis method can efficiently produce mesoporous N-doped carbon without using any corrosive

[a] Jieting Ding, Hui Wang, Prof Rongfang Wang  
State Key Laboratory Base for Eco-Chemical Engineering, College of Chemical Engineering  
Qingdao University of Science and Technology  
Qingdao (PR China)  
1358743525@qq.com; wangh@gust.edu.cn; rfwang@qust.edu.cn

[b] Prof Shan Ji  
College of Biological, Chemical Science and Chemical Engineering  
JiaXing University  
JiaXing (PR China)  
shan.ji@ucl.ac.uk

[c] Prof Bruno G. Pollet  
Department of Energy and Process Engineering, Faculty of Engineering

Norwegian University of Science and Technology  
Trondheim (Norway)

bruno.g.pollet@ntnu.no

Supporting information for this article is given via a link at the end of the document.

chemicals and complicated post-treatment processes. 3-dimensional network-like shape with large open porous structures was obtained by this method, and the CoS nanoparticles were evenly distributed in the carbon matrix. The electrochemical properties were effectively tuned via adjusting the mesoporous structures. In alkaline media,  $\text{Co}_{1-x}\text{S}/\text{NC}$  exhibited outstanding electrochemical properties which were comparable to those obtained for commercial Pt/C in HER and ORR in terms of electrochemical activity and durability.

## Results and Discussion

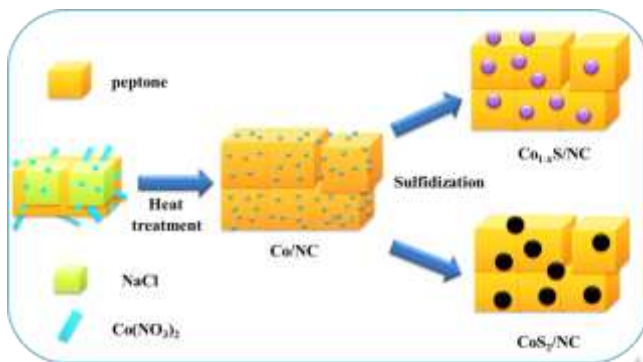


**Figure 1.** Schematic of the formation of  $\text{Co}_{1-x}\text{S}/\text{NC}$  and  $\text{CoS}_2/\text{NC}$ .

Figure 1 schematically represents the procedure of synthesizing  $\text{Co}_{1-x}\text{S}/\text{NC}$  and  $\text{CoS}_2/\text{NC}$ . There are principally two steps, namely carbonization and sulfidization. During the first step, peptone, a commercial and low-cost product, was used as carbon and nitrogen source, and was mixed with the Co precursor and NaCl template. Then the mixture was carbonized at 900 °C. The NaCl melted and formed nanodroplets in the mixture at that high temperature, which resulted in the formation of porous carbonized peptone. Because of using NaCl as a template, this method can significantly simplify the whole procedure and reduce the total cost, as this template can be easily removed by water rinsing. During the sulfidization, low-cost S powder was used as reagent and sulfidization was carried out hydrothermally in an autoclave. By adjusting the amount of S in the precursor, completely and partially sulfurized cobalt nanoparticles were obtained in the carbon matrix. The pictures of the samples in each step are presented in Figure S1.

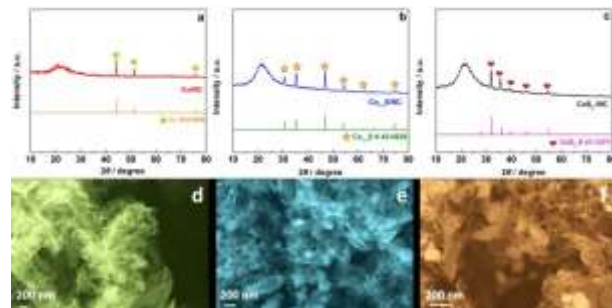


**Figure 2.** XRD patterns of Co/NC (a),  $\text{Co}_{1-x}\text{S}/\text{NC}$  (b) and  $\text{CoS}_2/\text{NC}$  (c); SEM images of Co/NC (d),  $\text{Co}_{1-x}\text{S}/\text{NC}$  (e) and  $\text{CoS}_2/\text{NC}$  (f).

XRD patterns of Co/NC,  $\text{Co}_{1-x}\text{S}/\text{NC}$  and  $\text{CoS}_2/\text{NC}$  are presented in Figure 2, where all samples show a broad and weak peak at ca.  $2\theta = 26^\circ$  corresponding to the (002) plane of graphitic carbon, implying that there is a small amount of graphite present in all three samples. As shown in Figure 2(a), the typical diffraction peaks of the face-centered cubic (fcc) Co (0) phase are observed at  $2\theta$  of  $44.28^\circ$ ,  $51.52^\circ$  and  $75.98^\circ$  corresponding to the (111), (200) and (220) planes respectively, confirming that metallic Co phase was obtained in the Co/NC sample. After sulfidization of Co/NC with S powder, Figure 2(b) shows that the characteristic peaks of a face-centered cubic (fcc) Co (0) phase were absent. Based upon the JCPDS No. 42-0826, the diffraction peaks at  $2\theta$  of  $30.61^\circ$ ,  $35.40^\circ$ ,  $46.72^\circ$ ,  $54.26^\circ$ ,  $62.38^\circ$  and  $74.42^\circ$  corresponding to the (100), (101), (102), (110), (103) and (202) planes of  $\text{Co}_{1-x}\text{S}$  are clearly present in the XRD pattern of  $\text{Co}_{1-x}\text{S}/\text{NC}$ . When the amount of S increased to 0.8 mmol in the precursors,  $\text{CoS}_2$  was formed as shown in Figure 2(c). The characteristic peaks of  $\text{CoS}_2$  are clearly shown in Figure 2(c) and based upon the JCPDS No. 41-1471, the diffraction peaks at  $2\theta$  of  $32.23^\circ$ ,  $36.2^\circ$ ,  $40.16^\circ$ ,  $46.38^\circ$  and  $55.22^\circ$  correspond to the (200), (210), (211), (220) and (311) planes. The XRD results indicate that cobalt exists in carbon matrix that can be efficiently sulfurized by this hydrothermal method.  $\text{Co}_{1-x}\text{S}$  and  $\text{CoS}_2$  could be controllably synthesized in the carbon by adjusting the amount of S powder in the precursors.

Figure 2(d-f) shows the SEM images of Co/NC,  $\text{Co}_{1-x}\text{S}/\text{NC}$  and  $\text{CoS}_2/\text{NC}$ . Compared to pure C sample (which was prepared by the same procedure without adding Co as precursor; the corresponding SEM image is presented in Figure S2 (a), Figure 2(d) shows that introducing  $\text{Co}(\text{NO}_3)_2$  in the precursor had no impact on the morphology of the obtained carbon. It was found that Co/NC had a sponge-like morphology with an open and porous structure after the NaCl template was removed by thorough water washing. Figure S2 (b) shows that NaCl plays a critical role in forming the porosity of the carbonized carbon material. Figure 2(d) shows that no visible particles can be observed. After Co/NC was hydrothermally sulfidized by S, Figure 2(e) shows that many large size particles were obtained, as presented in the SEM images, due to particle aggregation. When Co/NC was sulfurized by adding more S (0.8 mmol), a sponge-like morphology was formed as shown in the SEM

image, but many larger particles were formed due to the sulfurization process (Figure 2(f)). These SEM images suggest that sulfurization did not damage the structure of the carbon matrix, but Co particles were evenly distributed in the carbon matrix and aggregated to form much larger cobalt sulphides particles.

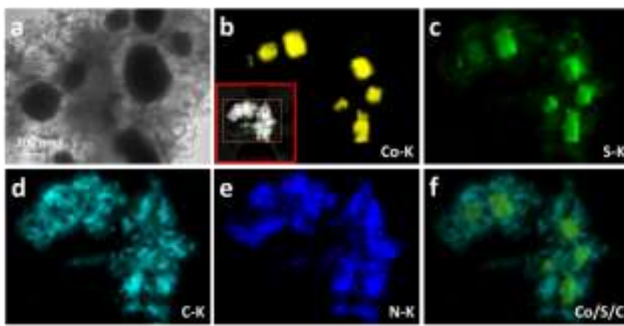


**Figure 3.** TEM image of  $\text{C}_{1-x}\text{S}/\text{NC}$  (a); STEM elemental mapping analysis of  $\text{C}_{1-x}\text{S}/\text{NC}$ , elements: Co (b), S (c), C (d), N (e) overlapped Co, S and C (f).

As shown in Figure S3, the Co nanoparticles with an average particle size of ca. 25 nm are uniformly dispersed in the carbon. However, the particle aggregation occurred when Co/NC was sulfurized by S. Figure 3(a) shows that much larger particles of a size of ca. 300 nm were produced. Beside the large black spots, many smaller irregular nanomaterials were also formed around the large and aggregated particles. The element distribution in  $\text{Co}_{1-x}\text{S}/\text{NC}$  was further evaluated by the STEM technique and its corresponding element mapping are presented in Figure 3(b-f). Figures 3(b) and 3(c) indicate that the Co and S elements were evenly dispersed in the cobalt sulfide particles. Figures 3(d) and 3(e) are the element distribution of C and N, which covered much larger area than the Co and S elements. The overlapped mapping image of Co/S/C (Figure 3(f)) confirmed that cobalt sulfide particles were covered by N-doped carbon.

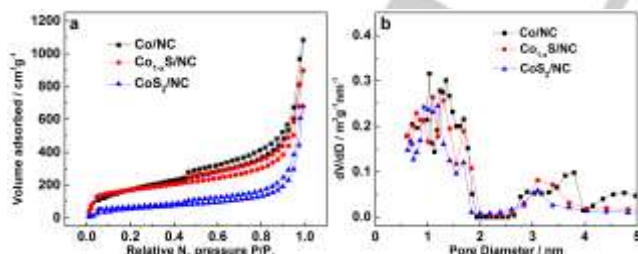


**Figure 4.**  $\text{N}_2$  adsorption and desorption isotherms of Co/NC,  $\text{Co}_{1-x}\text{S}/\text{NC}$  and  $\text{CoS}_2/\text{NC}$  (a); their corresponding pore size distributions (b).

The specific surface area and porosity of the as-prepared samples were analyzed by  $\text{N}_2$  adsorption-desorption isotherms. According to the IUPAC classification, the isotherms of all three samples correspond to mixed I/II type with a hysteresis loop in the relatively high-pressure region, indicating that meso-scaled pore existed in these samples. An uptake in the initial part of the

isotherms was observed, especially for Co/NC and  $\text{Co}_{1-x}\text{S}/\text{NC}$ , suggesting that micropores were also formed in the as-prepared samples. Figure 4(b) confirms the existence of micropore and mesopores in all three samples. The BET specific surface areas of Co/NC,  $\text{Co}_{1-x}\text{S}/\text{NC}$  and  $\text{CoS}_2/\text{NC}$  were calculated to be 1,050, 980 and 616  $\text{m}^2/\text{g}$ , respectively. This finding suggests that partial sulfurization did not have a significant impact on the surface area. However, when Co particles were fully sulfurized, a huge drop in the surface area was observed. As some small micropores are not accessible for reactants, it was deemed necessary to calculate the external surface area to evaluate the available surface area for reactants. Based upon the literature<sup>[4b, 13]</sup>, the external surface areas of Co/NC,  $\text{Co}_{1-x}\text{S}/\text{NC}$  and  $\text{CoS}_2/\text{NC}$  can be obtained via the V-t plot method as shown in Figure S4. The figure shows that the external surface area of  $\text{Co}_{1-x}\text{S}/\text{NC}$  was almost the same as that of Co/NC, and much higher than that of  $\text{CoS}_2/\text{NC}$ . Therefore, partial sulfurization of Co/NC did not affect the specific surface and external specific areas.

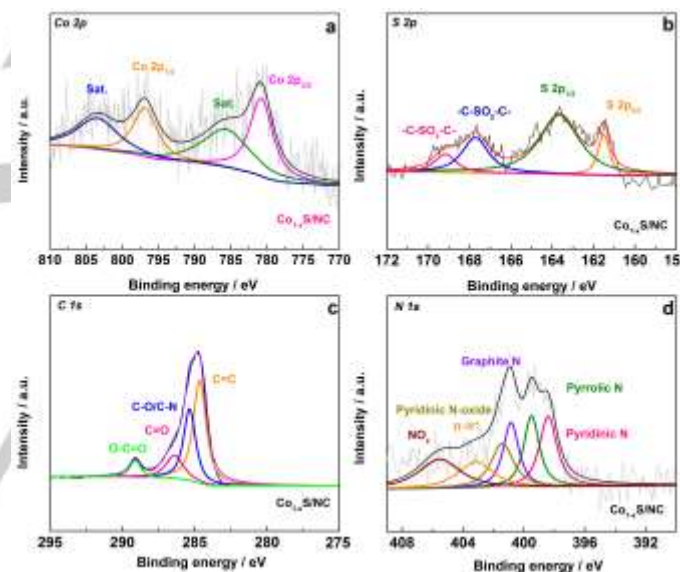


**Figure 5.** Deconvolution high-resolution XPS spectra of Co 2p (a), S 2p (b), C 1s (c) and N 1s (d) for  $\text{Co}_{1-x}\text{S}/\text{NC}$ .

X-ray photoelectron spectroscopy (XPS) was employed to investigate the surface composition and chemical states of  $\text{Co}_{1-x}\text{S}/\text{NC}$ . The XPS spectra of Co 2p is shown in Figure 5(a) in which the Co elements can be deconvoluted into two spin-orbit doublet containing low energy band Co 2p<sub>3/2</sub> and high energy band Co 2p<sub>1/2</sub> with two shake-up satellites, representing divalent Co element present in  $\text{Co}_{1-x}\text{S}/\text{NC}$ <sup>[14]</sup>. As shown in the deconvoluted S 2p spectra of  $\text{Co}_{1-x}\text{S}/\text{NC}$  in Figure 5(b), peaks at bonding energy of 161.3 and 163.7 eV correspond to metal-sulfur bonds and surficial sulfur ions at low coordination respectively<sup>[15]</sup>, and peaks at 167.8 and 169.3 eV are associated to S in C-SO<sub>2</sub>-C and C-SO<sub>3</sub>-C respectively<sup>[16]</sup>. As illustrated in Figure 5(c), C 1s XPS spectrum can be fitted into four peaks at

284.7, 285.4, 286.4 and 289.0 eV corresponding to  $\text{sp}^2$  C=C, C–O/C–N, C=O and O–C=O respectively<sup>[17]</sup>. It can be observed that most carbon species on the surface is  $\text{sp}^2$  C=C, in turn facilitating the electron transfer during the electrochemical reaction. C–O/C–N species shown in the C 1s XPS spectrum further confirms that the nitrogen atoms were doped into the carbon matrix. The N 1s XPS spectrum was fitted into six peaks, indicating there are six different nitrogen species existing in  $\text{Co}_{1-x}\text{S}/\text{NC}$ . These nitrogen species are: pyridinic-N at ca. 398.4 eV, pyrrolic-N at ca. 399.5 eV, graphitic-N at ca. 400.8 eV, pyridinic N-oxide at 401.4 eV,  $\pi$ - $\pi^*$  satellite at ca. 403.2 eV, and NO<sub>x</sub> at ca. 405.5 eV<sup>[18]</sup>. For the N-doped carbon materials, it is generally believed that pyridinic-N and pyrrolic-N can efficiently improve the electrocatalytic activity since pyridinic-N provides a pair of electrons to bond with p-conjugated rings and pyrrolic-N as a good electron donor<sup>[19]</sup>. Figure 5(d) clearly shows that the major nitrogen species on the surface of  $\text{Co}_{1-x}\text{S}/\text{NC}$  are pyrrolic N and pyridinic N.

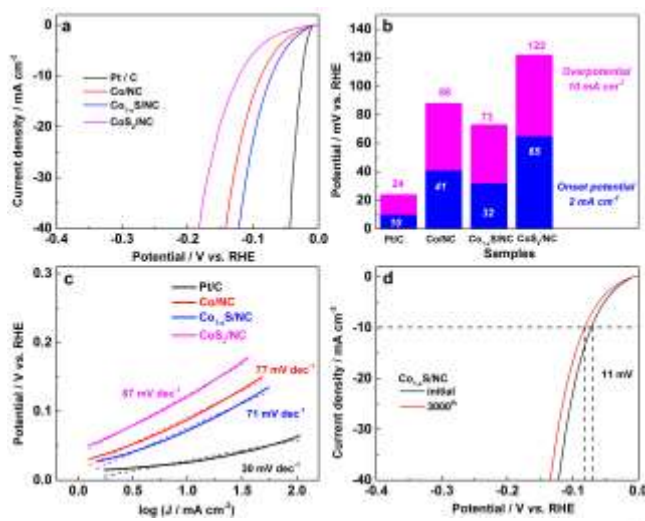


**Figure 6.** LSV polarization curves of HER tested on Pt/C, Co/NC,  $\text{Co}_{1-x}\text{S}/\text{NC}$  and  $\text{CoS}_2/\text{NC}$  electrodes (a); their corresponding HER overpotential (at 10 mA cm<sup>-2</sup>) and onset potentials (at 2 mA cm<sup>-2</sup>) (b); their HER Tafel plots (c); LSV polarization curves of HER at the first (1<sup>st</sup>) and 3,000<sup>th</sup> cycles tested on  $\text{Co}_{1-x}\text{S}/\text{NC}$  (d).

The electrocatalytic performance of the as-prepared samples for HER was evaluated by loading the catalyst materials on the rotating glassy carbon disc to avoid the effect of generated hydrogen. All results were also compared with the state-of-the-art commercial Pt/C catalyst (Pt, 20 wt.%) as shown in Figure 6(a). The figure shows that Pt/C exhibits superior HER activity when compared to the as-prepared CoS/C samples. Their corresponding overpotentials at 10 mA cm<sup>-2</sup> and onset potentials are shown in Figure 6(b). Among the as-prepared samples,  $\text{Co}_{1-x}\text{S}/\text{NC}$  exhibits the lowest HER overpotential with a value of 73 mV vs. RHE. It is observed that the HER overpotentials of Co/NC and  $\text{Co}_{1-x}\text{S}/\text{NC}$  are lower than that of Pt/C, but both of them have values smaller than 100 mV, making them viable as

HER catalyst for practical applications in water electrolyser. In order to investigate the HER processes occurring on these electrodes, the HER Tafel plots based upon the polarization curves of Pt/C, Co/NC,  $\text{Co}_{1-x}\text{S}/\text{NC}$  and  $\text{CoS}_2/\text{NC}$  electrodes were plotted as shown in Figure 6(c). There are three principal processes occurring during the HER, namely Volmer, Heyrovsky, and Tafel steps, which can be determined by the slopes of Tafel plots<sup>[20]</sup>. The slopes of Tafel plots for Pt/C, Co/NC,  $\text{Co}_{1-x}\text{S}/\text{NC}$  and  $\text{CoS}_2/\text{NC}$  were found to be 30, 77, 71 and 87 mV dec<sup>-1</sup>. Based upon the values of Tafel slopes, it was concluded that the HER occurring on the Co/NC,  $\text{Co}_{1-x}\text{S}/\text{NC}$  and  $\text{CoS}_2/\text{NC}$  electrodes followed a Volmer-Heyrovsky reaction, in other words, the electrochemical desorption was the rate-determining process in the whole HER. Since Co/NC and  $\text{Co}_{1-x}\text{S}/\text{NC}$  have similar specific surface area and pore size distribution, it can be concluded that the enhanced electrocatalytic activity of  $\text{Co}_{1-x}\text{S}/\text{NC}$  resulted from the sulfurized cobalt. The durability is a key parameter for HER catalysts. The Tafel slope and overpotential (at 10 mA cm<sup>-2</sup>) of  $\text{Co}_{1-x}\text{S}/\text{NC}$  was compared with some representative HER catalysts values found in the literature, as shown in Table S1, suggesting that  $\text{Co}_{1-x}\text{S}/\text{NC}$  is one of the best HER catalysts among these reported catalysts. The HER durability of these new materials was evaluated in 1.0 M KOH electrolyte by continuous cycles voltammetry (CV) for 3,000 cycles. The LSV plots of the 1<sup>st</sup> and 3,000<sup>th</sup> cycles on  $\text{Co}_{1-x}\text{S}/\text{NC}$  and Pt/C are shown in Figure 6(d) and Figure S5 respectively. These two figures clearly shows, for  $\text{Co}_{1-x}\text{S}/\text{NC}$  and Pt/C, overpotential shifts at a current density of 10 mA cm<sup>-2</sup> after 3,000 cycling of +11 mV and +32 mV respectively, indicating that  $\text{Co}_{1-x}\text{S}/\text{NC}$  is more stable in HER than Pt/C.

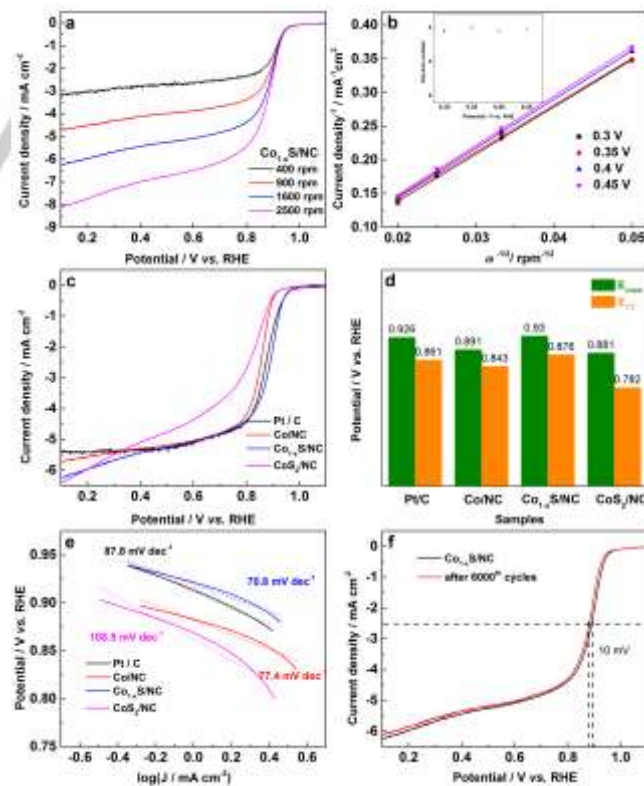


**Figure 7.** (a) LSV curves of  $\text{Co}_{1-x}\text{S}/\text{NC}$  on RDE in  $\text{O}_2$  saturated KOH solution at various rotation speeds; and (b) Koutecky-Levich plots of  $\text{Co}_{1-x}\text{S}/\text{NC}$  for ORR; (c) LSV curves for ORR on different catalysts; (d) onset potentials ( $E_{\text{onset}}$ ) and half-wave potentials ( $E_{1/2}$ ) for ORR on different catalysts; (e) corresponding ORR Tafel plots; (f) ORR LSV curves of the first (1st) and 6,000th cycle on  $\text{Co}_{1-x}\text{S}/\text{NC}$ .

Linear sweep voltammetry (LSV) for ORR was carried out on  $\text{Co}_{1-x}\text{S}/\text{NC}$  at various rotation speeds in an  $\text{O}_2$ -saturated KOH electrolyte. Figure 7(a) shows that the diffusion limiting current ( $i_{\text{lim}}$ ) was obtained when the potential was lower than +0.8 V vs. RHE. Figure 7(b) shows the Koutecky-Levich (K-L) plots, obtained from the polarization curves at various potentials, were straight lines and almost overlapped with each other, implying that the ORR occurring on  $\text{Co}_{1-x}\text{S}/\text{NC}$  was a first-order reaction (for dissolved  $\text{O}_2$ )<sup>[21]</sup>. The electron transfer number during the ORR was also calculated based upon the slope of  $i^1$  plotted vs.  $\omega^{1/2}$ . The inset of Figure 7(b) shows the ORR on  $\text{Co}_{1-x}\text{S}/\text{NC}$  involves a highly efficient four-electron transfer process. Corresponding electrochemical measurements were also carried out for Pt/C, Co/NC and  $\text{CoS}_2/\text{NC}$  as shown in Figure S6. The ORR on Pt/C and Co/NC also followed a four-electron transfer process, but  $\text{CoS}_2/\text{NC}$  did not. The ORR polarization curves of the as-prepared catalysts were compared with that of Pt/C in Figure 7(c), and their corresponding onset potentials ( $E_{\text{onset}}$  : potential at a current density of  $-0.2 \text{ mA cm}^{-2}$ ) and half-wave potentials ( $E_{1/2}$ ) are shown in Figure 7(d). The figure clearly shows that  $\text{Co}_{1-x}\text{S}/\text{NC}$  is the most active catalysts toward ORR among all the tested catalysts, including the state-of-the-art commercial Pt/C in terms of  $E_{1/2}$  (Pt/C: +0.861 V vs. RHE,  $\text{Co}_{1-x}\text{S}/\text{NC}$ : +0.876 V vs. RHE). The ORR performance of the as-prepared and Pt/C samples were further evaluated by comparing their Tafel slopes as shown in Figure 7(e). Based upon the mass-transport corrected Tafel (MTCT) plots, the Tafel slopes of Pt/C, Co/NC,  $\text{Co}_{1-x}\text{S}/\text{NC}$  and  $\text{CoS}_2/\text{NC}$  were found to be 87.8, 77.4, 70.8 and  $108.5 \text{ mV dec}^{-1}$  respectively.  $\text{Co}_{1-x}\text{S}/\text{NC}$  shows the lowest Tafel slope among all the tested samples, indicating it has the best reaction kinetics for ORR. The ORR durability of the best as-prepared catalyst ( $\text{Co}_{1-x}\text{S}/\text{NC}$ ) against Pt/C was further evaluated by continuous CV for 6,000 cycles in KOH electrolyte. Their corresponding LSV curves of the 1<sup>st</sup> and 6,000<sup>th</sup> cycles are shown in Figure 7(f) and Figure S7(a). It was found that the  $E_{1/2}$  of  $\text{Co}_{1-x}\text{S}/\text{NC}$  negatively shifted by +10 mV after 6,000 cycles, and for Pt/C, it shifted by +44 mV, in other words, in our conditions,  $\text{Co}_{1-x}\text{S}/\text{NC}$  exhibited a much better ORR durability than Pt/C in a KOH electrolyte. After the durability test, the morphology of the  $\text{Co}_{1-x}\text{S}/\text{NC}$  was studied by SEM. As shown in Figure S7(b), no visible difference could be found after the 6,000 cycling test when compared to the fresh  $\text{Co}_{1-x}\text{S}/\text{NC}$  shown in Figure 2. A comparison of  $\text{Co}_{1-x}\text{S}/\text{NC}$  with previously reported and representative non-precious metal ORR electrocatalysts is shown in Table S2, highlighting that  $\text{Co}_{1-x}\text{S}/\text{NC}$  is one of the best ORR catalysts.

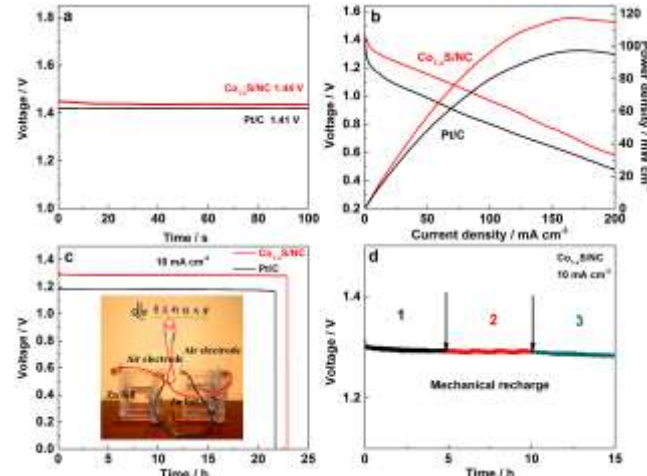


**Figure 8.** (a) Open circuit voltage (OCV) of  $\text{Co}_{1-x}\text{S}/\text{NC}$  and Pt/C primary zinc-air batteries; (b) Polarization and power density curves of  $\text{Co}_{1-x}\text{S}/\text{NC}$  and Pt/C primary Zn-air batteries; (c) cell voltage vs. time at the current density of  $10 \text{ mA cm}^{-2}$ , the inset photograph of a red LED (2 V) powered by two liquid Zn-air batteries with the  $\text{Co}_{1-x}\text{S}/\text{NC}$  air cathode connected in series; (d) long-term galvanostatic discharge of  $\text{Co}_{1-x}\text{S}/\text{NC}$  primary Zn-air battery, which had been recharged by refilling Zn foil for three times.

To further evaluate its ORR performance in ‘real’ world conditions,  $\text{Co}_{1-x}\text{S}/\text{NC}$  was used as an ORR catalyst and assembled into a primary Zn-air battery. Figure 8(a) shows that the open cell voltage (OCV) of a  $\text{Co}_{1-x}\text{S}/\text{NC}$  cell was 1.44 V, exhibiting excellent stability, and its OCV was higher than that of a Pt/C cell. Polarization and power density curves of the  $\text{Co}_{1-x}\text{S}/\text{NC}$  and Pt/C cells were plotted as shown in Figure 8(b). The figure shows that the  $\text{Co}_{1-x}\text{S}/\text{NC}$  cell delivered a power density of  $119 \text{ mW cm}^{-2}$  at a current density of  $150 \text{ mA cm}^{-2}$ , a much higher value than that of a Pt/C cell ( $97 \text{ mW cm}^{-2}$ ). When the  $\text{Co}_{1-x}\text{S}/\text{NC}$  and Pt/C cells were discharged at a current density of  $10 \text{ mA cm}^{-2}$ , the operating cell voltage of the  $\text{Co}_{1-x}\text{S}/\text{NC}$  cell was 1.28 V, higher than that of Pt/C, i.e. 1.18 V, and the  $\text{Co}_{1-x}\text{S}/\text{NC}$  cell could be discharged at this current density for 22.9 hours, whereas the Pt/C cell lasted for 21.6 hours. As shown in the inset of Figure 8(c), two  $\text{Co}_{1-x}\text{S}/\text{NC}$  cells were connected in series to power a 2 V LED red light, and the LED light was lit for more than 16 hours. Generally, primary Zn-air cells can be “recharged” by refilling the consumed Zn foil and electrolyte. After “recharging” three times, Figure 8(d) shows a slight decrease in operating voltage at a current density of  $10 \text{ mA cm}^{-2}$  after each “recharge”, further proving that  $\text{Co}_{1-x}\text{S}/\text{NC}$  has excellent stability for ORR in the primary Zn-air cell. The high ORR activity and durability of  $\text{Co}_{1-x}\text{S}/\text{NC}$  could result from the strong coupling and synergistic effect between cobalt sulfides and carbon matrix, making it a promising non-precious metal alternative to Pt/C for ORR.

## Conclusions

A low-cost and efficient method to produce cobalt sulfide/N-doped carbon compounds with open structure interconnected by carbon sheets by using NaCl as template during the carbonizing process was successfully developed. The obtained catalyst

showed remarkably high HER and ORR bifunctional electrocatalytic performances. The optimized  $\text{Co}_{1-x}\text{S}/\text{NC}$  samples outperformed most of the transition metal-based HER catalysts reported in the literature, and their ORR performances were even better than state-of-the-art commercial Pt/C in terms of activity and durability. Moreover,  $\text{Co}_{1-x}\text{S}/\text{NC}$  was also assembled into a primary Zn-air battery to evaluate its ORR performance in a real-world environment. It was found that the zinc-air battery containing the new catalyst material delivered a high-power density at ca. 119 mW cm<sup>-2</sup> (at a current density of 150 mA cm<sup>-2</sup>), higher than that a Zn-air cell containing Pt/C. This newly developed electrocatalytic material shows great potential as HER and ORR bifunctional catalysts for green energy conversion technologies and beyond.

## Experimental Section

**Synthesis:** Analytical grade chemicals were used all throughout this study without any further purification. The CoS/NC samples were synthesized via a two-step process, described as follows: In the first step, 0.2 g of  $\text{Co}(\text{NO}_3)_2 \cdot 6\text{H}_2\text{O}$  were dissolved in 15 mL of  $\text{H}_2\text{O}$ . After  $\text{Co}(\text{NO}_3)_2$  was completely dissolved, 1 g of peptone (biochemical reagent, CAS number: 73049-73-7, grade: R.) was added to this solution and magnetically stirred for 30 min. The obtained mixture was then freeze-dried with liquid nitrogen. The freeze-dried samples were mixed with 10 g NaCl and then ball-milled at 4,000 rpm for 6 h. The milled mixtures were placed in an inert gas tube furnace and carbonized at 900 °C for 1 h and at a heating rate of 2.5 °C min<sup>-1</sup>. The carbonized samples were thoroughly washed with ultrapure water to remove the NaCl template and dried in a vacuum oven. The obtained samples were labelled as Co/NC. In the second step, 0.2 mmol and 0.8 mmol of S powders were separately dissolved in a mixed solution containing 10 ml of ethanol and 10 ml of ethylenediamine, and then 0.05 g of the obtained Co/NC sample was introduced to the above solutions. The obtained solutions were transferred into a Teflon-lined stainless-steel autoclave. The autoclave was heated at 180 °C for 12 h. After cooling to room temperature, the obtained samples were washed with ultrapure water and then dried in a vacuum oven at 60 °C for 12 h. The obtained samples were labelled as  $\text{Co}_{1-x}\text{S}/\text{NC}$  (0.2 mmol S powders) and  $\text{CoS}_2/\text{NC}$  (0.8 mmol S powders).

**Physical Characterization:** XRD patterns of the catalysts were recorded on a Shimadzu XD-3A (Japan), using filtered Cu-K $\alpha$  radiation ( $\lambda = 0.15418 \text{ nm}$ ), generated at 40 kV and 30 mA. Scans for 2 $\theta$  values were recorded at 4° min<sup>-1</sup> between 25° and 90°. Transmission electron micrographs (TEM) were taken on a JEOL (JEM-2000 FX) microscope operating at 200 kV. Energy dispersive spectroscopy (EDS) was employed for determining the elemental composition. The specific surface area was determined by Brunauere-Emmette-Teller (BET) method and the pore size distribution was calculated by the density functional theory (DFT) method using the model (slit pore, NLDFT equilibrium model) on a Quantachrome Autosorb-1 volumetric analyzer. X-ray photoelectron spectra (XPS) was acquired with a VG Escalab210 spectrometer fitted with Mg 300 W X-ray source.

**Electrochemical measurements:** HER and ORR electrochemical performance tests were carried out in a conventional three-electrode cell on a CHI650D electrochemical analyzer (CH Instruments). The working electrode was prepared as follows: 5 mg of the catalyst were dispersed into 1 mL Nafion® ethanol solution (0.25 wt.%) by ultrasonic mixing for 30 min. 8  $\mu\text{L}$  of ink (containing 40  $\mu\text{g}$  catalyst) were dropped onto the surface of a polished glass carbon rotating disc electrode (catalyst loading = 0.204 mg cm<sup>-2</sup>) and dried in air. For comparison purposes,

commercial Pt/C catalysts were also prepared as working electrodes using the same procedure. Either a Hg/HgO (1 M KOH) or a Ag/AgCl (saturation KCl) were chosen as reference electrodes, and a graphitic rod/ Pt wire as a counter electrode. The electrolyte solutions (1 M KOH and 0.1M KOH) were purged with  $\text{N}_2$  for 30 min for all electrochemical experiments in this study. All potentials used in this work were converted to potentials versus the reversible hydrogen electrode (RHE) by using the following equations:

$$\text{ERHE} = \text{E}_{\text{Hg/HgO}} + 0.059 \text{ pH} + 0.14 \text{ V} \quad (1)$$

$$\text{ERHE} = \text{E}_{\text{Ag/AgCl}} + 0.059\text{pH} + 0.197 \text{ V} \quad (2)$$

iR compensation was applied to all the electrochemical measurements.

As-prepared carbon materials were used as cathodes and Zn foil as an anode in a two-electrode cell system. In order to precisely measure specific capacity, Zn foil electrode was tailored to a 1 cm<sup>2</sup> surface area, smoothened and polished before each test. The air cathode was prepared by dispersing 2 mg of the catalyst, 3  $\mu\text{L}$  of polymer binder PTFE, 1 mg acetylene black and 4 mg carbon in 300  $\mu\text{L}$  isopropyl alcohol to form a homogenous slurry. After rolling into a slice and oven drying at 80 °C, the air cathode mixture was pressed onto Ni foam under 20 MPa.

## Acknowledgements

The authors would like to thank the National Natural Science Foundation of China (21766032 and 51661008)

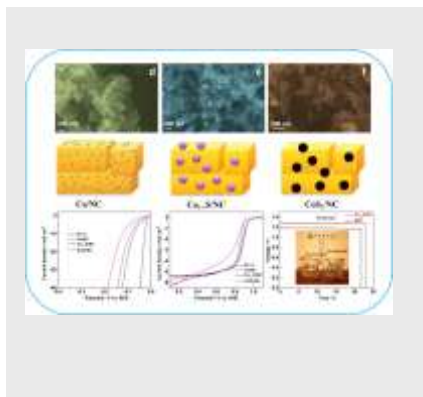
**Keywords:** Cobalt sulphide • Mesoporous carbon • Hydrogen evolution reaction • Oxygen reduction reaction • Bifunctional catalyst

- [1] a) Y. Yan, B. Xia, B. Zhao, X. Wang, *J. Mater. Chem. A* **2016**, *4*, 17587-17603; b) M. Zhou, H. L. Wang, S. Guo, *Chem. Soc. Rev.* **2016**, *45*, 1273-1307; c) M. Lefèvre, E. Proietti, F. Jaouen, J. P. Dodelet, *Science* **2009**, *324*, 71-74; d) T. Meng, J. Qin, S. Wang, D. Zhao, B. Mao, M. Cao, *J. Mater. Chem. A* **2017**, *5*, 7001-7014.
- [2] a) Y. Jiao, Y. Zheng, M. Jaroniec, S. Z. Qiao, *Chem. Soc. rev.* **2015**, *44*, 2060-2086; b) X. Cui, P. Ren, D. Deng, J. Deng, X. Bao, *Energy Environ. Sci.* **2016**, *9*, 123-129.
- [3] a) Yanguang Li, Hongjie Dai, *Chem. Soc. Rev.* **2014**, *43*, 5257-5275; b) W. Tian, H. Li, B. Qin, Y. Xu, Y. Hao, Y. Li, G. Zhang, J. Liu, X. Sun, X. Duan, *J. Mater. Chem. A* **2017**, *5*, 7103-7110.
- [4] a) R. Wang, T. Zhou, H. Wang, H. Feng, S. Ji, *J. Power Sources* **2014**, *269*, 54-60; b) J. Ding, S. Ji, H. Wang, J. Key, D. J. L. Brett, R. Wang, *J. Power Sources* **2018**, *374*, 48-54.
- [5] A. Sumboja, J. Chen, Y. Zong, P. S. Lee, Z. Liu, *Nanoscale* **2017**, *9*, 774-780.
- [6] J. Yin, Y. Li, F. Lv, Q. Fan, Y. Q. Zhao, Q. Zhang, W. Wang, F. Cheng, P. Xi, S. Guo, *ACS Nano* **2017**, *11*, 2275-2283.
- [7] J. Shi, J. Hu, Y. Luo, X. Sun, A. M. Asiri, *Cata. Sci. Technol.* **2015**, *5*, 4954-4958.
- [8] M. Shun, W. Zhenhai, C. Suqin, G. Xiaoru, O. Kostya, C. Junhong, *Small* **2015**, *11*, 414-419.
- [9] J. Wang, D. Gao, G. Wang, S. Miao, H. Wu, J. Li, X. Bao, *J. Mater. Chem. A* **2014**, *2*, 20067-20074.
- [10] X. Qiao, S. Liao, R. Zheng, Y. Deng, H. Song, L. Du, *ACS Sustain. Chem. Eng.* **2016**, *4*, 4131-4136.
- [11] G. Nam, J. Park, M. Choi, P. Oh, S. Park, M. G. Kim, N. Park, J. Cho, J.-S. Lee, *ACS Nano* **2015**, *9*, 6493-6501.
- [12] D. Jiao, R. Pengju, D. Dehui, B. Xinhe, *Angew. Chem. Int. Ed. Engl.* **2015**, *54*, 2100-2104.
- [13] J. Ding, S. Ji, H. Wang, B. G. Pollet, R. Wang, *Electrochim. Acta* **2017**, *255*, 55-62.
- [14] G. He, M. Qiao, W. Li, Y. Lu, T. Zhao, R. Zou, B. Li, J. A. Darr, J. Hu, M. M. Titirici, *Adv. Sci.* **2017**, *4*, 1600214.
- [15] Q. Liu, Z. Wu, Z. Ma, S. Dou, J. Wu, L. Tao, X. Wang, C. Ouyang, A. Shen, S. Wang, *Electrochim. Acta* **2015**, *177*, 298-303.
- [16] L. Pan, H. Zhang, L. Li, Z. Yan, D. Ju, C. Xu, H. Ning, W. Yu, *Acs Appl. Mater. Interfaces* **2017**, *9*, 2500-2508.
- [17] a) D.-S. Liu, D.-H. Liu, B.-H. Hou, Y.-Y. Wang, J.-Z. Guo, Q.-L. Ning, X.-L. Wu, *Electrochim. Acta* **2018**, *264*, 292-300; b) Q. Gan,

- [18] H. He, K. Zhao, Z. He, S. Liu, *Electrochim. Acta* **2018**, *266*, 254-262.  
a) H. Liu, Y. Zhang, R. Li, X. Sun, S. Désilets, H. Abou-Rachid, M. Jaidann, L.-S. Lussier, *Carbon* **2010**, *48*, 1498-1507; b) R. Arrigo, M. Havecker, R. Schlogl, D. S. Su, *Chem. Commun.* **2008**, 4891-4893.  
[19] a) Y. Qiu, X. Zhang, S. Yang, *Phy. Chem. Chem. Phy.* **2011**, *13*, 12554-12558; b) D. Hulicova-Jurcakova, M. Kodama, S. Shiraishi, H. Hatori, Z. H. Zhu, G. Q. Lu, *Adv. Fun. Mater.* **2009**, *19*, 1800-1809.  
M. Li, X. Liu, Y. Xiong, X. Bo, Y. Zhang, C. Han, L. Guo, *J. Mater. Chem. A* **2015**, *3*, 4255-4265.  
R. Zhang, C. Zhang, W. Chen, *J. Mater. Chem. A* **2016**, *4*, 18723-18729.

**FULL PAPER****WILEY-VCH****FULL PAPER**

Herein, highly efficient mesoporous CoS/N-doped carbon materials was developed as HER and ORR electrocatalysts for water splitting and zinc-air batteries. The obtained sulphide (CoS)/carbon materials showed open structures composed of interconnected thin carbon nanosheets with transition metal-based nanoparticles wrapped inside the carbon matrix.



Jieting Ding, Shan Ji,\* Hui Wang, Bruno G. Pollet, Rongfang Wang\*

**Mesoporous CoS/N-doped Carbon as HER and ORR Bifunctional Electrocatalyst for Water Electrolyzers and Zinc-Air Batteries**

Accepted Manuscript